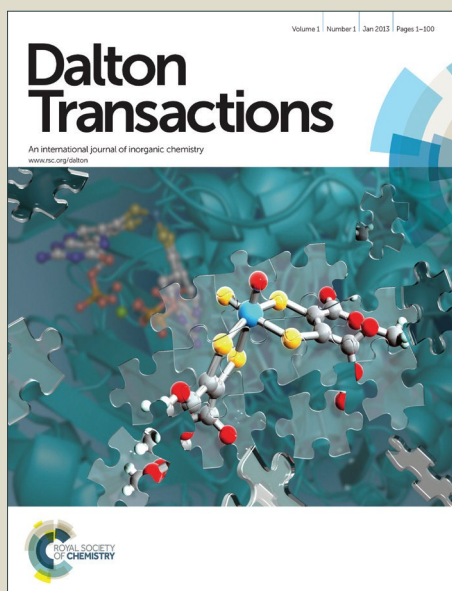


# Dalton Transactions

Accepted Manuscript



This article can be cited before page numbers have been issued, to do this please use: Y. Wang, L. Chen, C. Liu, Z. Du, L. Chen and Q. Liu, *Dalton Trans.*, 2016, DOI: 10.1039/C6DT00676K.



This is an *Accepted Manuscript*, which has been through the Royal Society of Chemistry peer review process and has been accepted for publication.

*Accepted Manuscripts* are published online shortly after acceptance, before technical editing, formatting and proof reading. Using this free service, authors can make their results available to the community, in citable form, before we publish the edited article. We will replace this *Accepted Manuscript* with the edited and formatted *Advance Article* as soon as it is available.

You can find more information about *Accepted Manuscripts* in the [Information for Authors](#).

Please note that technical editing may introduce minor changes to the text and/or graphics, which may alter content. The journal's standard [Terms & Conditions](#) and the [Ethical guidelines](#) still apply. In no event shall the Royal Society of Chemistry be held responsible for any errors or omissions in this *Accepted Manuscript* or any consequences arising from the use of any information it contains.



Journal Name

ARTICLE

## 3D Chiral and 2D achiral cobalt(II) compounds constructed of 4-(benzimidazole-1-yl)benzoic Ligand exhibiting field-induced single-ion-magnet-type slow magnetic relaxation

Received 00th January 20xx,  
Accepted 00th January 20xx

DOI: 10.1039/x0xx00000x

www.rsc.org/

Yu-Ling Wang,<sup>a</sup> Lin Chen,<sup>a</sup> Cai-Ming Liu,<sup>b</sup> Zi-Yi Du,<sup>c</sup> Li-Li Chen<sup>a</sup> and Qing-Yan Liu<sup>\*a</sup>

Organizing magnetically isolated 3d transition metal ions, which behave as single-ion magnets (SIMs) units, in a coordination network is a promising approach to design novel single-molecule magnets (SMMs). Herein a 3D chiral and a 2D achiral cobalt(II) coordination compounds based on the single metal nodes with the 4-(benzimidazole-1-yl)benzoic acid (Hbmzbc) ligand, namely, [Co(bmzbc)<sub>2</sub>(1, 2-*etdio*)]<sub>n</sub> (**1**) (1, 2-*etdio* = 1, 2-ethanediol) and [Co(bmzbc)<sub>2</sub>(Hbmzbc)]<sub>n</sub> (**2**), have been synthesized and structurally characterized. The 3D chiral structure **1** with 2-fold interpenetrating *qtz* topological nets consisting of totally achiral components was obtained via spontaneous resolution. While achiral structure **2** is a 2D (4, 4) net. In both structures, the individual cobalt(II) ions are spatially well separated by the long organic ligands in the well-defined networks. Magnetic measurements on **1** and **2** showed field-induced slow magnetic relaxation resulting from single-ion anisotropy of the individual Co(II) ions. Analysis of the dynamic ac susceptibilities with Arrhenius law afforded the anisotropy energy barrier of 16.8(3) and 31.3(2) K under a 2 kOe static magnetic field for **1** and **2**, respectively. The distinct coordination environments of the Co(II) ions in **1** and **2** lead to the different anisotropic energy barriers.

### Introduction

In the field of molecule-based magnetic materials much effort has so far been concentrated on the area of single-molecule magnets (SMMs),<sup>1</sup> which demonstrate slow relaxation of magnetic moments after removing an external magnetic field, with potential applications in magnetic information storage, quantum computation and spintronics.<sup>2</sup> The large ground-state spin *S* and zero-field splitting parameter *D*, which give the high relaxation energy barriers ( $U_{\text{eff}}$ ), are the prerequisites for a molecule to be a SMM.<sup>3</sup> Thus the polynuclear compounds based on the high-spin 3d metal ions have afforded the most diversity of the SMMs.<sup>4</sup> However, a single lanthanide ion-based SMM, which is referred to as a single-ion magnet (SIM), with a high energy barrier has been documented in 2003.<sup>5</sup> The 4f and 5f metal ions-based SIMs display slow magnetic relaxation resulting from a large ground-state spin and a strong easy-axis magnetic anisotropy for these metal ions.<sup>6</sup> Very recently, the exploration of new SIMs has been extended to 3d transition-metal ions. A few examples of SIMs based on

the Fe(II),<sup>7</sup> Fe(III),<sup>8</sup> Mn(II),<sup>9</sup> Co(II)<sup>10</sup> ions have been reported due to their single-ion anisotropy. On the other hand, the association of polynuclear SMM unit into coordination networks has provided a unique approach to create new SMMs.<sup>11</sup> Could slow magnetic relaxation occur in coordination networks containing magnetically isolated 3d transition metal ions? Actually, very recently two cobalt(II) coordination polymers exhibiting slow magnetic relaxation have been documented.<sup>12</sup> This type of slow magnetic relaxation arises from an individual metal ion in a certain ligand field, which is a typical SIM. Thus the design of SIMs can be achieved by organizing magnetic ions with suitable local magnetic anisotropy into polymeric architectures, which can be considered as a promising approach to a new generation of molecular magnetic materials. For metal ions behaving as SIM units in a well-defined network, it requires long connections between the magnetic centers to avoid the magnetic interaction. Following this approach, we synthesized a large spatial ligand of 4-(benzimidazole-1-yl)benzoic acid (Hbmzbc). It should be noted that the synthetic method for this organic ligand (Scheme S1) is totally different from the reported one.<sup>13</sup> The Hbmzbc ligand has a large skeleton with the coordination donors of N and O atoms are spatially separated, which can effectively separate the metal centers from each other. In addition, the Hbmzbc ligand is suitable as a bridging ligand that can exhibit an adaptable conformation in a certain structure as a result of the free rotation of the C–N single bond between the benzene moiety and benzimidazole moiety. Reaction of CoCl<sub>2</sub>·6H<sub>2</sub>O and Hbmzbc in different solvents afforded two compounds, [Co(bmzbc)<sub>2</sub>(1, 2-*etdio*)]<sub>n</sub> (**1**) and

<sup>a</sup> College of Chemistry and Chemical Engineering, Jiangxi Normal University, Nanchang, Jiangxi 330022, P. R. China. E-mail: qyliu@chem@hotmail.com.

<sup>b</sup> Beijing National Laboratory for Molecular Sciences, Institution of Chemistry, Chinese Academy of Sciences, Center for Molecular Sciences, Beijing 100190, P. R. China.

<sup>c</sup> College of Chemistry and Chemical Engineering, Gannan Normal University, Ganzhou 341000, P. R. China.

Electronic Supplementary Information (ESI) available: X-ray crystallographic data in CIF format, materials and methods, figures of structure, XRPD, and TGA curve and magnetic data. CCDC-1443010 and 1422328. For ESI and crystallographic data in CIF or other electronic format See DOI: 10.1039/x0xx00000x

## ARTICLE

Journal Name

[Co(bmzbc)<sub>2</sub>(Hbmzbc)]<sub>n</sub> (**2**). Compounds **1** and **2** exhibit different structural dimensionalities with chiral 3D and achiral 2D structures, respectively, demonstrating the adaptable character of the Hbmzbc ligand. Detailed magnetic studies show that **1** and **2** exhibit field-induced slow magnetic relaxation wherein the single Co(II) ion behave as a SIM unit in the polymeric structures.

## Results and discussion

### Syntheses

It is well-known that the reaction solvent plays an important role in the formation of the final crystalline products. In the present case, reactions of CoCl<sub>2</sub>·6H<sub>2</sub>O and Hbmzbc in different solvents lead to different structures. Using the 1, 2-ethanediol (1,2-*etdio*) solvent with high viscosity, 3D structure of **1** was obtained. Single-crystal X-ray diffraction analyses revealed that **1** crystallizes in the chiral trigonal space group *P*3<sub>1</sub>21 (Table 1). The Flack parameter is  $-0.005(6)$ , which is nearly zero, indicating that each individual crystal of **1** consists of a single enantiomer. However, there is no chiral source in the reaction mixture. Thus, the overall ensemble of the crystals in a batch of **1** can be expected to be racemic, which indicates that spontaneous resolution occurred during crystal growth. The solid-state circular dichroism (CD) spectra for samples obtained from two separately synthetic batches further confirmed the racemic of the bulk material of **1** (Fig. 1). With aqueous solvent in the similar reaction a 2D achiral structure of **2** was obtained, which indicates that the final outcomes are significantly affected by the reaction medium. Furthermore, a 2D compound {[Co(bmzbc)<sub>2</sub>·2DMF]<sub>n</sub>} exhibiting interesting adsorption properties and slow magnetic relaxation has been reported by our group very recently, which was obtained using the DMF as the solvent.<sup>14</sup>

### Structural description

The asymmetric unit of **1** consists of half a Co(II) ion, one bmzbc<sup>-</sup> anion, and half a 1, 2-*etdio* molecule with a 2-fold rotation axis symmetry. As depicted in Fig. 2, the Co(II) ion located on a 2-fold rotation axis is six-coordinated by two benzimidazole N atoms from two bmzbc<sup>-</sup> ligands and two hydroxyl O atoms of a 1, 2-*etdio* in a square-planar geometry, with the Co–N and Co–O bond lengths of 2.095(2) to 2.167(2) Å, respectively (Table 2). The two axial positions of the [CoN<sub>2</sub>O<sub>4</sub>] octahedron are occupied by two carboxylic O (O1A and O1B) atoms from another two bmzbc<sup>-</sup> ligands (Co–O = 2.0887(18) Å). The bmzbc<sup>-</sup> ligand bridges two Co(II) ions through the monodentate carboxylic and benzimidazole groups with the dihedral angle between benzene ring and benzimidazole ring of 69.69° (Scheme S2). The 1, 2-*etdio* coordinates to one Co(II) ion in a chelating fashion with its two hydroxyl groups. The octahedral Co(II) ions are linked by the bmzbc<sup>-</sup> ligands to generate a 3D framework as shown in Fig. 3a. It is interesting that in the 3D structure the Co(II) ions are bridged by bmzbc<sup>-</sup> ligands to form an infinite left-handed

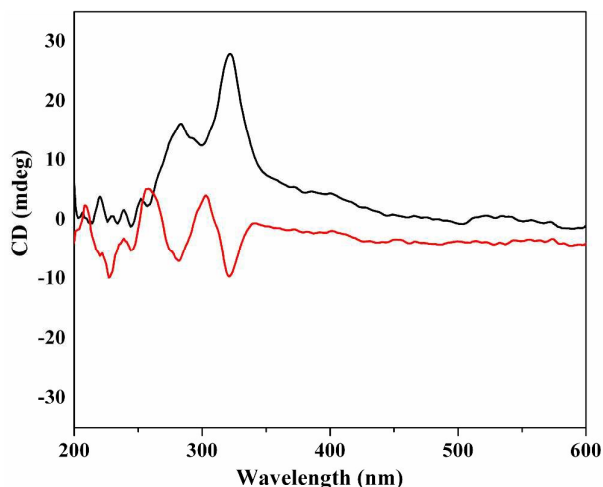
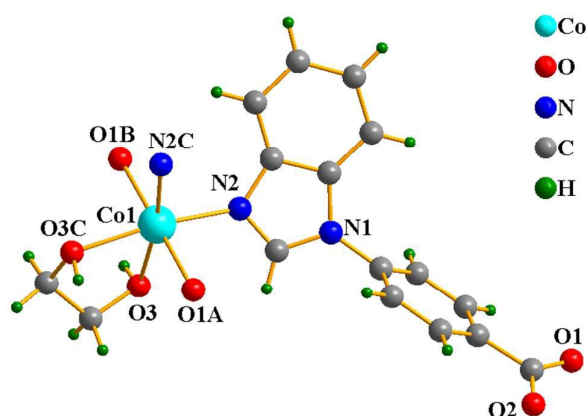


Fig. 1 The Solid-state CD spectra for two synthetic batches of bulk samples **1**.

Table 1 Crystal data and structural refinements for **1** and **2**.

Empirical formula	C <sub>30</sub> H <sub>24</sub> N <sub>4</sub> O <sub>6</sub> Co	C <sub>42</sub> H <sub>28</sub> N <sub>6</sub> O <sub>6</sub> Co
Formula weight	595.46	771.63
Crystal system	Trigonal	Triclinic
Space group	<i>P</i> 3 <sub>1</sub> 21	<i>P</i> -1
<i>a</i> (Å)	12.9013(4)	11.7983(7)
<i>b</i> (Å)	12.9013(4)	11.9044(7)
<i>c</i> (Å)	15.3095(9)	14.4291(8)
$\alpha$ /deg	90	72.807(3)
$\beta$ /deg	90	81.143(3)
$\gamma$ /deg	120	61.863(2)
<i>V</i> /Å <sup>3</sup>	2206.78(19)	1706.98(18)
<i>Z</i>	3	2
<i>D</i> <sub>calcd</sub> /g cm <sup>-3</sup>	1.344	1.501
$\mu$ /mm <sup>-1</sup>	0.631	0.565
<i>F</i> (000)	921	794
Independent reflections	3324	7849
Observed reflections. [ <i>I</i> > 2 $\sigma$ ( <i>I</i> )]	2861	7173
<i>R</i> [int]	0.0209	0.0201
GOF on <i>F</i> <sup>2</sup>	1.009	1.003
2 $\theta$ range[°]	1.823 to 27.455	1.477 to 27.647
<i>R</i> <sub>1</sub> , <i>wR</i> <sub>2</sub> [ <i>I</i> > 2 $\sigma$ ( <i>I</i> )]	0.0286, 0.0771	0.0305, 0.0836
<i>R</i> <sub>1</sub> , <i>wR</i> <sub>2</sub> (all data)	0.0396, 0.0919	0.0340, 0.0866
Largest diff. Peak and hole[e·Å <sup>-3</sup> ]	0.354 and -0.233	0.287 and -0.293

helical chain running along the *c*-axis (Fig. 3b). The helix is generated around the crystallographic 3<sub>1</sub> screw axis. Additionally, the 3D structure contains the double-stranded right-handed helical chains running along the *c* axis to give 1D helical channels (Fig. 3c), which indicates that the structure **1** has the hexagonal pseudo-6<sub>1</sub> symmetry (Fig. 3a). All indicate structure **1** has a chiral  $\alpha$ -quartz (**qtz**) topology.<sup>15</sup> Indeed, each Co(II) ion is bridged by four bmzbc<sup>-</sup> ligands in a bidentate



**Fig. 2** The coordination environment of the Co(II) center (Symmetric codes: A  $x - y + 1, -y + 1, -z + 2/3$ ; B  $-y + 1, x - y + 1, z - 2/3$ ; C  $y, x, -z$ ).

**Table 2** Selected bond distances (Å) and bond angles(°).

Compound 1		Compound 2	
Co1–O1A	2.0887(18)	Co1–N6	2.0875(11)
Co1–O1B	2.0887(18)	Co1–O6A	2.1040(10)
Co1–N2C	2.095(2)	Co1–O1	2.1045(10)
Co1–N2	2.095(2)	Co1–N4B	2.1562(12)
Co1–O3	2.167(2)	Co1–O3	2.1571(10)
Co1–O3C	2.167(2)	Co1–O5A	2.2384(10)
O1A–Co1–O1B	179.51(14)	N6–Co1–O1	91.46(5)
O1A–Co1–N2C	86.71(9)	O6A–Co1–O1	104.35(4)
O1B–Co1–N2C	93.62(10)	N6–Co1–N4B	93.93(5)
O1A–Co1–N2	93.62(9)	O6A–Co1–N4B	95.08(5)
O1B–Co1–N2	86.71(9)	O1–Co1–N4B	87.43(4)
N2C–Co1–N2	95.96(15)	N6–Co1–O3	85.84(4)
O1A–Co1–O3	90.43(8)	O6A–Co1–O3	83.34(4)
O1B–Co1–O3	89.19(9)	O1–Co1–O3	99.59(4)
N2–Co1–O3	92.58(10)	N4B–Co1–O3	172.98(4)
O1A–Co1–O3C	89.1799	N6–Co1–O5A	103.62(4)
O1B–Co1–O3C	90.43(8)	O6A–Co1–O5A	60.69(4)
N2C–Co1–O3C	92.58(10)	N4B–Co1–O5A	91.79(4)
O3–Co1–O3C	78.98(14)	O3–Co1–O5A	81.46(4)

Symmetric codes: **1**, A  $x - y + 1, -y + 1, -z + 2/3$ ; B  $-y + 1, x - y + 1, z - 2/3$ ; C  $y, x, -z$ . **2**, A  $x, y - 1, z$ ; B  $x - 1, y + 1, z$ .

bridging fashion, which bridge the Co(II) ions to form the 3D structure. Thus structure **1** can be reduced into a chiral **qtz** topological net based on the 4-connected cobalt nodes with the Schläfli symbol of  $6^4 \cdot 8^2$  (Fig. 4). With Co...Co separation of 12.34(3) Å, a large void is generated within a single **qtz** net (Fig. 3a). Therefore structural interpenetration is difficult to avoid for such an empty framework. Actually, the void space in **1** is filled by the formation of two independent **qtz** nets. The closest Co...Co separation between the two interpenetrating nets is 8.61(5) Å, indicating a spatially separated the Co(II) centers. Careful investigation showed that the two mutually interpenetrated chiral **qtz** networks have the same handedness (Fig. 4b), which is different from that of the recently reported Zn(II) compound with the same ligand.<sup>16</sup> In that Zn(II) compound, two enantiomeric **qtz** nets are mutually interpenetrated. The formation of these **qtz** nets indicates the tetrahedral metal node and the adaptive linear 4-(benzimidazol-1-yl)benzoic rod with the feasible conformations facilitate the construction of the chiral **qtz** net.

Compound **2** crystallizes in a triclinic *P*-1 space group (Table 1). One Co(II) ion and three crystallographically independent 4-(benzimidazole-1-yl)benzoic ligands are in the asymmetric unit of **2**. There should be an organic ligand with protonated

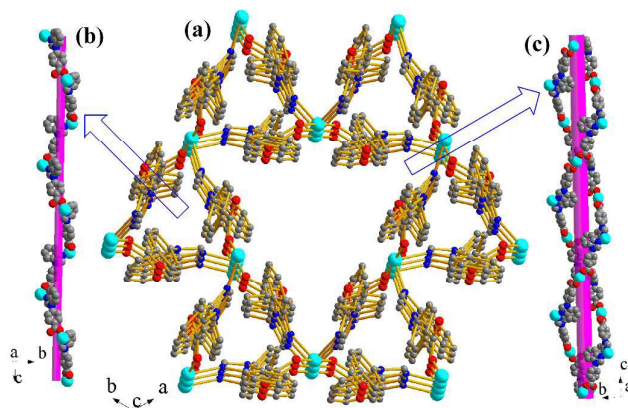


**Fig. 3** (a) 3D framework of **1** (The 1, 2-ethdio molecules are omitted for clarity). (b) the left-handed helix in **1**. (c) the chiral channel formed by double right-handed helix in **1**.

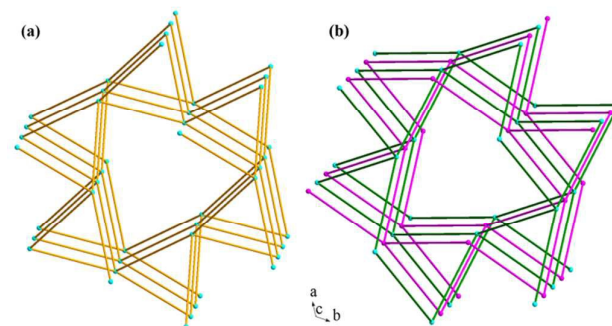


**Fig. 4** (a) A single **qtz** net of **1** and (b) 2-fold interpenetrating **qtz** network with same handedness in **1** discriminated by colors.

## ARTICLE

Journal Name

carboxylic group for charge balance, as suggested by the strong absorption at  $1700\text{ cm}^{-1}$  in the IR spectrum. The carboxylic hydrogen atom was added at the O4 atom due to the much different C21–O4 ( $1.2824(19)\text{ \AA}$ ) and C21–O3 ( $1.2302(17)\text{ \AA}$ ) bond distances and strong H-assisted hydrogen bond between the carboxylic groups ( $\text{O4}\cdots\text{O2} = 2.4389(16)\text{ \AA}$ ). The Co(II) atom is bonded to four carboxylic O atoms from two  $\text{bmzbc}^-$  ligands and one Hbmzbc ligand, and two benzimidazole N atoms from the second Hbmzbc ligand and the third  $\text{bmzbc}^-$  ligand (Fig. 5). The four equatorial positions of Co(II) are occupied by three carboxylic O (O1, O5A and O6A) and a N6 atoms; O3 and N4B take up the apical positions to complete the octahedral coordination geometry of each Co center. The Co–O bond distances vary from  $2.1040(10)$  to  $2.2383(10)\text{ \AA}$  with the longest bond distance associated with the chelating carboxylic group (Table 2). The Co–N bond distances are  $2.0875(11)$  and  $2.1561(12)\text{ \AA}$ . The axial O–Co–N bond angle of  $172.98(4)^\circ$  and the equatorial O/N–Co–O/N bond angles ranging from  $60.69(4)$  to  $104.36(4)^\circ$  all deviate from the corresponding angles of  $180$  and  $90^\circ$ , respectively, for an ideal octahedron.

The three independent organic ligands exhibit three types of coordination modes (Scheme S2). One of the  $\text{bmzbc}^-$  ligand as a terminal ligand monodentately coordinated to a Co(II) ion through a carboxylic oxygen and the other  $\text{bmzbc}^-$  ligand bridges two Co(II) ions through its chelating carboxylic group and the monodentate benzimidazole N atom. The Hbmzbc bridges two Co(II) ions through its one monodentate carboxylic O and the benzimidazole N atoms. As depicted in Fig. 5, each Co(II) ion is surrounded by five organic ligands, four of which link the Co(II) ions to give a 2D (4,4) net with metal-organic squares (Fig. 6). The 2D layer is extended along the  $ab$  plane. Within the metal-organic squares, the Co $\cdots$ Co separations are

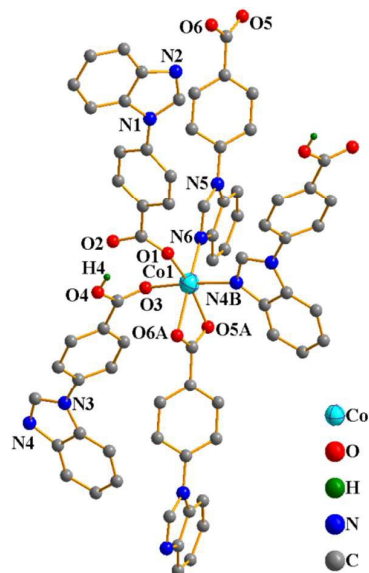


**Fig. 5** The coordination environment of the Co(II) ion in **2** (Symmetric codes: A  $x, y - 1, z$ ; B  $x - 1, y + 1, z$ ).

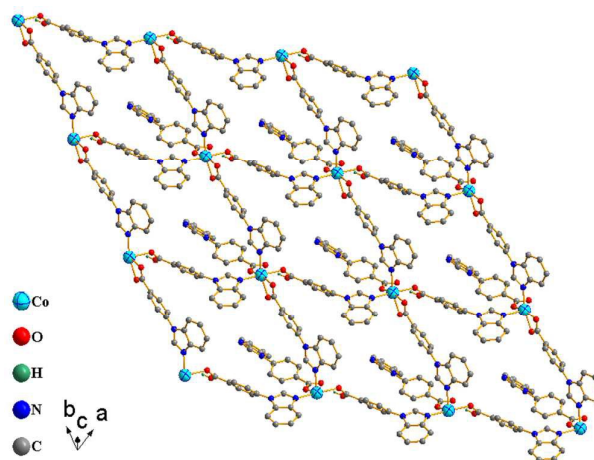


**Fig. 6** The 2D layered structure of **2**.

$11.9$  and  $12.1\text{ \AA}$ , affording nanosized square cavities. It is interesting that the terminal  $\text{bmzbc}^-$  ligands as suspensions hang at one side of the layer (Fig. S1). In the crystal packing, two neighboring layers are interdigitated with each other through the hanging  $\text{bmzbc}^-$  ligands penetrating into the nanosized cavities of the metal-organic squares (Fig. S2). Each nanosized cavity is enough to encapsulate one  $\text{bmzbc}^-$  ligand from neighboring layer. The two interdigitated layers are packed along the  $c$  direction to generate a 3D packing (Fig. S3). Examination of the 3D packing indicates the closest interlayered Co $\cdots$ Co separation is  $7.73\text{ \AA}$ , which suggests an isolated magnetic environment for the Co(II) ion.

In structure **2**, the three crystallographically independent organic ligands exhibit three kinds of conformations with the dihedral angles between benzene ring and benzimidazole ring are  $47.7, 50.8, 53.2^\circ$ , respectively, demonstrating the diverse conformations for this organic ligand. It should be noted that the compound **2** is not a common (4,4) net constructed from the single metal ion surrounded by four bridging organic ligands, as observed in its reported cobalt(II) and zinc(II) compounds with the  $\text{bmzbc}^-$  ligand.<sup>14,17</sup> In **2**, the single metal ion is surrounded by four bridging organic ligands to form the (4,4) network and an additional terminal  $\text{bmzbc}^-$  ligand to fill the cavity of the neighboring (4,4) network. Thus a novel structure is generated.

#### IR spectra, thermogravimetric analyses and powder X-ray diffraction patterns

In the IR spectra of **1** and **2**, the strong bands between  $1651$  and  $1459\text{ cm}^{-1}$  can be attributed to the stretching bands of carboxylic groups of  $\text{bmzbc}^-$  ligand. The broad band centered at  $3474\text{ cm}^{-1}$  in the IR spectrum of **1** can be assigned to the O–H stretching band of the 1, 2-ethanediol. The C–O stretching band of the 1, 2-ethanediol is appeared at  $1238\text{ cm}^{-1}$  in the IR spectrum of **1**. The strong peak at  $1700\text{ cm}^{-1}$  in the IR spectrum of **2** indicates the presence of the protonated carboxylic group of the Hbmzbc in **2**. The phase purity of the bulky samples of **1** and **2** were checked by the powder X-ray

diffraction (PXRD). As shown in Fig. S4, the experimental PXRD patterns match well with the simulated ones calculated from single-crystal diffraction data, indicative of the single phase of both materials. The thermal behavior of **1** and **2** were investigated by the thermogravimetric analyses (TGA) (Fig. S5). TGA curve of **1** exhibits two weight loss steps. The first weight loss of 13.81% between 110 to 260 °C can be assigned to the loss of the 1, 2-ethanediol molecule (calcd. 10.43%) and the 1, 2-ethanediol solvent attached at the surface of the crystals. The decomposition of the framework of **1** occurs at 400 °C. The 2D compound **2** is robust and stable up to 318 °C. Above this temperature, the collapse of the organic ligand starts.

### Magnetic properties

The magnetic susceptibilities of **1** and **2** were measured in a direct-current (dc) field of 1 kOe in the temperature range of 2–300 K. The plots of  $\chi_M T$  ( $\chi_M$  is the molar magnetic susceptibility per Co(II)) versus  $T$  are depicted in Fig. 7. At 300 K, the  $\chi_M T$  values are 3.10 and 2.94 cm<sup>3</sup> K mol<sup>-1</sup>, which are significantly larger than the expected value of 1.875 cm<sup>3</sup> K mol<sup>-1</sup> for an isotropic Co(II) ion ( $S = 3/2$  and  $g_0 = 2.0$ ). However, the values are within the range of those observed for compounds containing the high-spin Co(II) with an unquenched angular momentum.<sup>18</sup> The effective  $g_{\text{eff}} = 2.53$  and 2.50 for **1** and **2**, respectively, can be deduced from the room temperature  $\chi_M T$  value, which are larger than the spin-only value of  $g_0 = 2.0$ , suggesting the considerable orbital contributions to the spin-only value. As the temperature is lowered, the  $\chi_M T$  products decrease slowly between 300–100 K and fall sharply to a minimum of 2.01 and 1.84 cm<sup>3</sup> K mol<sup>-1</sup> at 2 K for **1** and **2**, respectively, revealing the occurrence of significant spin-orbit coupling. The isothermal magnetization measurements of **1** and **2** were measured at different temperatures. For **1**,  $M$  vs  $H/T$  plots are not superimposed (Figure 7a insert). For **2**, the bifurcation of the  $M$  vs  $H/T$  plots appears to be more significant (Fig. 7b insert), especially at lower temperatures and higher field range, confirming the presence of significant magnetic anisotropy, which is attributed to the strong spin-orbital coupling of the Co(II) ion.

As described above, the closest Co...Co separations in **1** and **2** are 8.61 and 7.73 Å, respectively. Thus, the magnetic interaction between the local spin quartets can be negligible. So the individual Co(II) ions in **1** and **2** maybe behave as a SIM unit that will exhibit slow magnetic relaxation. In order to investigate the dynamic magnetic behaviour of **1** and **2**, the temperature dependencies of the alternating-current (ac) magnetic susceptibilities of **1** and **2** were collected at zero dc field with an ac field of 2.5 Oe with oscillating frequencies. The results are given in Fig. S6 in the form of  $\chi'$  and  $\chi''$  versus  $T$  plots ( $\chi'$  and  $\chi''$  are the in-phase and out-of-phase ac molar magnetic susceptibilities, respectively). No frequency dependent signal can be observed under zero dc field in the measurements, indicative of a fast tunnelling of the magnetization (QTM). In addition, the  $M$  vs  $H$  data for **1** and **2** do not exhibit a hysteresis effect from MPMS measurements at 1.9 K used in a

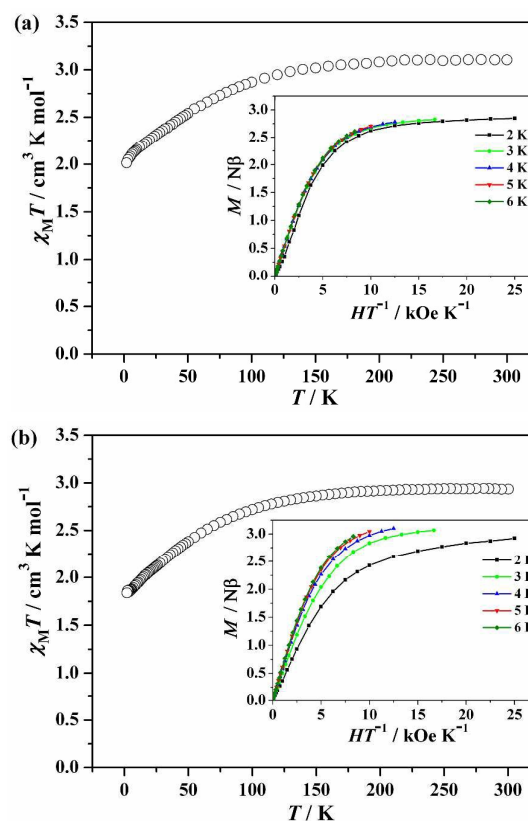
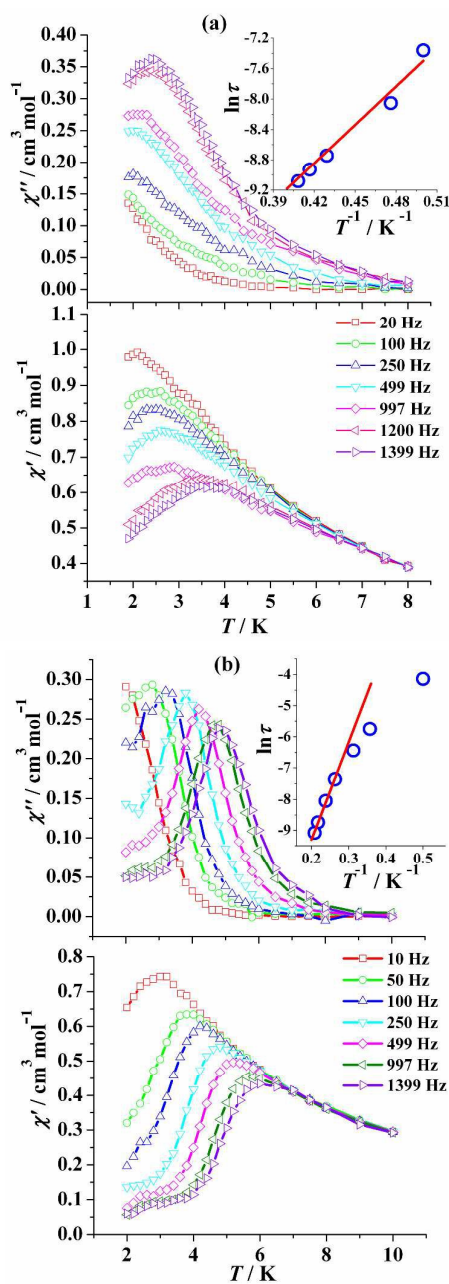


Fig. 7 The  $\chi_M T$  versus  $T$  plots for **1** (a) and **2** (b). Inset: Experimental  $M$  versus  $H/T$  plots at different temperatures.

traditional SQUID magnetometer (Fig. S7), verifying the QTM effect for **1** and **2**.

The application of a dc field of 2 kOe suppresses the QTM and the temperature- and frequency- dependence of  $\chi'$  and  $\chi''$  are observed for **1** and **2** in the test frequencies (Fig. 8), which is the typical for a field-induced SIM. As shown in Fig. 8a, the peak of the  $\chi''$  can be detected in **1** when the frequency larger than 250 Hz. While for **2**, full peaks of the  $\chi''$  can be observed in the frequency larger than 10 Hz. Analysis of the frequency dependence of the  $\chi''$  peaks through Arrhenius law ( $\tau = \tau_0 \exp(U_{\text{eff}}/kT)$ , where  $T$  is the temperature of the maximum  $\chi''$  at different frequencies,  $\tau = 1/2\pi\nu$ , and  $U_{\text{eff}}$  is the anisotropic energy barrier) afforded an anisotropic energy barrier of 16.8(3) K (11.6(8) cm<sup>-1</sup>) with a pre-exponential factor  $\tau_0$  of  $1.2(2) \times 10^{-7}$  s for **1** and 31.3(2) K (21.7(6) cm<sup>-1</sup>) with a pre-exponential factor  $\tau_0$  of  $1.7(3) \times 10^{-7}$  s for **2**, respectively (Fig. 8 insert). The  $U_{\text{eff}}$  values are slightly lower than that of 1D cobalt(II)-triazole compound under 1.5 kOe (31.6 cm<sup>-1</sup>),<sup>12a</sup> but higher than that of dicyanamide-bridged 2D cobalt(II) compound under 1 kOe (5.1 cm<sup>-1</sup>).<sup>12b</sup> The value of the pre-exponential factor  $\tau_0$  is within the typical range for SIMs ( $1 \times 10^{-7}$  to  $1 \times 10^{-11}$  s).

The Cole-Cole plots at 2 K under the 2 kOe dc field were generated from the frequency-dependent ac susceptibility data for **1**. The Cole-Cole diagram in the form of  $\chi''$  versus  $\chi'$  is



**Fig. 8** Temperature dependence of the out-of phase and in-phase ac susceptibility signals under 2 kOe dc field for **1** (a) and **2** (b). Inset: Magnetization relaxation time,  $\ln \tau$  vs.  $T^{-1}$  plot under 2 kOe dc field. The solid line is fitted with the Arrhenius law.

shown in Fig. S8, which displays a large semicircle accompanying with a small semicircle. This implies that two relaxation processes are present in **1**. The Cole–Cole curve was fitted by the sum of two modified Debye functions (equ S1).<sup>19</sup> However, the data is not fitted well with the Debye function (Fig. S8). For **2**, the Cole–Cole plots at 2, 3 and 4 K in the 2 kOe dc field were plotted in Fig. 9. Two-step thermal magnetic relaxation character was also observed in the Cole–Cole plots

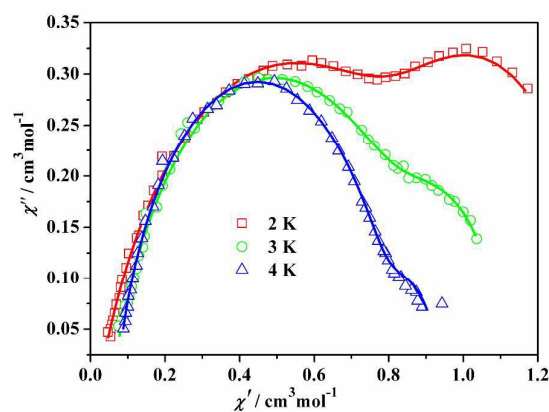


**Fig. 9** Cole-Cole plots for **2** under 2 kOe dc field. The solid lines are the best fit obtained with a sum of two modified Debye functions Debye model.

wherein the left and right parts correspond to the fast relaxation phase (FR) and the slow relaxation phase (SR), respectively. The Cole–Cole curves could be well fitted by the sum of two modified Debye functions. The fitting results are depicted in Fig. 9 and Fig. S9. The resulting  $\alpha_1$  values varying from 0.000005 to 0.0249 are much smaller than the  $\alpha_2$  values ranging 0.285 to 0.156 at all three temperatures (Table S1). These values suggest that the FR phase has a narrower distribution of the relaxation time in comparison to the SR phase. As mentioned above, there is only one kind of Co(II) ion in **1** and **2**, so the field-inducing role is ascribed to the two-step magnetic relaxation.<sup>20</sup> Such a behavior is similar to the two relaxation peaks observed in a mononuclear Dy-based SIM.<sup>21</sup>

## Experimental

### Materials and Instrumentations.

All commercially available chemicals are of reagent grade and used as received without further purification. IR (KBr pellets) spectra were recorded in the 400–4000  $\text{cm}^{-1}$  range using a Perkin-Elmer Spectrum One FT-IR spectrometer. Elemental analyses were carried out on Elementar Perkin-Elmer 2400CHN microanalyzer. Thermogravimetric analyses were carried out on a PE Diamond TG/DTA unit at a heating rate of 10  $^{\circ}\text{C}/\text{min}$  under a nitrogen atmosphere. Powder X-ray diffraction patterns were performed on a Rigaku Miniflex II powder diffractometer using Cu-K $\alpha$  radiation ( $\lambda = 1.5418 \text{ \AA}$ ). The  $2\theta$  range was 5–60 $^{\circ}$  with a continuous scan step width of 0.05 $^{\circ}$ . The recorded PXRD patterns were compared with theoretical patterns calculated from single-crystal structure data. Magnetic measurements were carried out on crystalline samples with a Quantum Design MPMS-XL5 SQUID magnetometer in the temperature range of 2–300 K. Diamagnetic corrections were estimated from Pascal's constants for all constituent atoms.<sup>22</sup>

### Synthesis.

The Hbmzbc ligand was prepared following a modified known procedure (Scheme S1).<sup>23</sup>

**Synthesis of [Co(bmzbc)<sub>2</sub>(1, 2-*etdio*)<sub>n</sub> (1).** CoCl<sub>2</sub>·6H<sub>2</sub>O (0.0119 g, 0.05 mmol), 4-(benzimidazol-1-yl)benzoic acid ligand (0.0238 g, 0.1 mmol) and triethylamine (0.05 mL) were mixed in 5 mL 1, 2-ethanediol solvent. The resulting mixture was sealed in a Teflon-lined stainless steel autoclave and heated at 120 °C for 72 h. Then the mixture allowed to cool to room temperature naturally to obtain the red crystals of **1** (yield: 0.0152 g, 50% on the basis of Co). Anal. calcd. for C<sub>30</sub>H<sub>24</sub>N<sub>4</sub>O<sub>6</sub>Co (595.46): C, 60.51; H, 4.06; N, 9.41%. Found: C, 58.68; H, 4.31; N, 9.19%. Main IR features (KBr pellet, cm<sup>-1</sup>): 3474 (m), 3145 (w), 2958 (w), 2521 (w), 1938 (w), 1604 (s), 1546 (m), 1516 (m), 1481 (w), 1459 (s), 1392 (s), 1322 (m), 1299 (m), 1238 (s), 1175 (w), 1140 (w), 1091 (w), 1074 (m), 1045 (w), 1014 (w), 989 (m), 934 (w), 910 (w), 870 (m), 831 (m), 792 (s), 778 (w), 748 (s), 726 (w), 704 (s), 648 (m), 620 (m), 585 (m), 561 (w), 532 (m), 491 (m), 427 (w).

**Synthesis of [Co(bmzbc)<sub>2</sub>(Hbmzbc)]<sub>n</sub> (2).** A mixture of CoCl<sub>2</sub>·6H<sub>2</sub>O (0.0119 g, 0.05 mmol) and 4-(benzimidazole-1-yl)benzoic acid (0.0357 g, 0.15 mmol) in 5 mL H<sub>2</sub>O was sealed in a 25 mL Parr Teflon-lined stainless steel vessel. The vessel was sealed and heated to 140 °C. This temperature was kept for 5 days and then the mixture was cooled naturally to form red block crystals of **2** (yield: 0.0166 g, 43% on the basis of Co). Anal. calcd. for C<sub>42</sub>H<sub>28</sub>N<sub>6</sub>O<sub>6</sub>Co (771.63): C, 65.37; H, 3.66; N, 10.89%. Found: C, 65.41; H, 3.69; N, 10.83%. Main IR features (cm<sup>-1</sup>, KBr pellet): 3854 (w), 3421 (m), 3121 (w), 3057 (w), 2517 (w), 1934 (w), 1700 (s), 1651 (s), 1605 (s), 1547 (s), 1518 (m), 1481 (s), 1426 (m), 1325 (m), 1297(m), 1236 (s), 1173 (w), 1147 (w), 1135 (w), 1102 (w), 1012 (m), 986 (m), 967 (w), 938 (w), 909 (m), 866 (s), 838 (w), 790 (s), 743 (s), 719 (w), 700(s), 643 (m), 622(m), 586 (s), 554 (w), 528 (m), 490 (m), 430 (w).

#### Crystallography.

Single crystal X-ray diffraction data of compounds **1** and **2** were collected on a Bruker Apex II CCD diffractometer equipped with a graphite-monochromated Mo-K $\alpha$  radiation ( $\lambda$  = 0.71073 Å). Data reduction was performed using SAINT and corrected for Lorentz and polarization effects. Adsorption corrections were applied using the SADABS routine.<sup>24</sup> The structures were solved by the direct methods and successive Fourier difference syntheses, and refined by the full-matrix least-squares method on  $F^2$  (SHELXTL Version 5.1).<sup>25</sup> All non-hydrogen atoms are refined with anisotropic thermal parameters. Hydrogen atoms attached to the C atoms and the carboxylic hydrogen atoms were assigned to calculated positions. The alcohol hydrogen were located from difference maps and refined with isotropic thermal parameters fixed at 1.5 times that of the respective oxygen atoms in **1**. The  $R_1$  values are defined as  $R_1 = \sum ||F_o| - |F_c|| / \sum |F_o|$  and  $wR_2 = \{\sum [w(F_o^2 - F_c^2)^2] / \sum [w(F_o^2)^2]\}^{1/2}$ . The details of the crystal parameters, data collection, and refinement are summarized in Table 1 and the selected bond distances and angles are listed in Table 2.

## Conclusions

In conclusion, a 3D chiral compound with 2-fold interpenetrating **qtz** network and a 2D achiral compound with (4,4) network based on the cobalt(II) nodes and Hbmzbc ligand have been synthesized and characterized. In both structures, the six-coordinate Co(II) ions are well isolated from each other *via* the long organic bridging ligands. Both compounds exhibit field-induced slow relaxation consistent with SIM behavior, which enriches the 3d transition-metal SIMs. This work demonstrates that slow magnetic relaxation can be observed in the high-dimensional Co(II) coordination networks wherein the highly anisotropic central Co(II) ions are in an isolated magnetic environment and behave as SIM units. This approach will provide a new route to the design molecular magnetic material based on a mononuclear complex unit.

## Acknowledgements

This work was supported by the NNSF of China (Grants 21561015, 21361011 and 21101081), the Provincial NSF of Jiangxi (Grant 20151BAB203002), and the Young Scientist Training Project of Jiangxi Province (Grant 20153BCB23017).

## Notes and references

- D. Gatteschi, R. Sessoli and J. Villain, *Molecular Nanomagnets*; Oxford University Press, 2006.
- (a) *Molecular Magnets: Physics and Applications*; J. Bartolomé, F. Luis and J. F. Fernandez, Eds.; Springer-Verlag: Berlin, 2014; (b) G. Aromí, D. Aguilá, P. Gamez, F. Luis and O. Roubeau, *Chem. Soc. Rev.*, 2012, **41**, 537–546.
- R. Sessoli, D. Gatteschi, A. Caneschi and M. A. Novak, *Nature*, 1993, **365**, 141–143.
- (a) M. Murrie, *Chem. Soc. Rev.*, 2010, **39**, 1986–1995; (b) X. -Y. Wang, C. Avendanño and K. R. Dunbar, *Chem. Soc. Rev.*, 2011, **40**, 3213–3238.
- N. Ishikawa, M. Sugita, T. Ishikawa, S. Koshihara and Y. Kaizu, *J. Am. Chem. Soc.*, 2003, **125**, 8694–8695.
- (a) L. Sorace, C. Benelli and D. Gatteschi, *Chem. Soc. Rev.*, 2011, **40**, 3092–3104. (b) D. N. Woodruff, R. E. P. Winpenny and R. A. Layfield, *Chem. Rev.*, 2013, **113**, 5110–5148. (c) F. Habib and M. Murugesu, *Chem. Soc. Rev.*, 2013, **42**, 3278–3288; (d) P. Zhang, Y. -N. Guo and J. K. Tang, *Coord. Chem. Rev.*, 2013, **257**, 1728–1763; (e) M. -H. Zeng, Y. Zheng, Y. -X. Tan, W. -X. Zhang, Y. -P. He and M. Kurmoo, *J. Am. Chem. Soc.* 2014, **136**, 4680–4688.
- (a) D. E. Freedman, W. H. Harman, T. D. Harris, G. J. Long, C. J. Chang and J. R. Long, *J. Am. Chem. Soc.*, 2010, **132**, 1224–1225; (b) P. -H. Lin, N. C. Smythe, S. J. Gorelsky, S. Maguire, N. J. Henson, I. Korobkov, B. L. Scott, J. C. Gordon, R. T. Baker and M. Murugesu, *J. Am. Chem. Soc.*, 2011, **133**, 15806–15809; (c) D. Weismann, Y. Sun, Y. Lan, G. Wolmershäuser, A. K. Powell and H. Sitzmann, *Chem. Eur. J.*, 2011, **17**, 4700–4704; (d) J. M. Zadrozny, M. Atanasov, A. M. Bryan, C. -Y. Lin, B. D. Reinken, P. P. Power, F. Neese and J. R. Long, *Chem. Sci.*, 2013, **4**, 125–138.
- S. Mossin, B. L. Tran, D. Adhikari, M. Pink, F. W. Heinemann, J. -P. Sutter, R. K. Szilagyi, K. Meyer and D. J. Mindiola, *J. Am. Chem. Soc.*, 2012, **134**, 13651–13661.
- (a) J. Vallejo, A. Pascual-Álvarez, J. Cano, I. Castro, M. Julve, F. Lloret, J. Krzystek, G. De Munno, D. Armentano, W. Wernsdorfer, R. Ruiz-García and E. Pardo, *Angew. Chem.*,

## ARTICLE

## Journal Name

- Int. Ed.*, 2013, **52**, 14075–14079; (b) R. Ishikawa, R. Miyamoto, H. Nojiri, B. K. Breedlove and M. Yamashita, *Inorg. Chem.*, 2013, **52**, 8300–8302; (c) A. Grigoropoulos, M. Pissas, P. Papatolis, V. Psycharis, P. Kyritsis and Y. Sanakis, *Inorg. Chem.*, 2013, **52**, 12869–12871.
- 10 (a) T. Jurca, A. Farghal, P.-H. Lin, I. Korobkov, M. Murugesu and D. S. Richeson, *J. Am. Chem. Soc.*, 2011, **133**, 15814–15817; (b) J. M. Zadrozny and J. R. Long, *J. Am. Chem. Soc.*, 2011, **133**, 20732–20734; (c) F. Habib, O. R. Luca, V. Vieru, M. Shiddiq, I. Korobkov, S. I. Gorelsky, M. K. Takase, L. F. Chibotaru, S. Hill, R. H. Crabtree and M. Murugesu, *Angew. Chem., Int. Ed.*, 2013, **52**, 11290–11293; (d) S. Gómez-Coca, E. Cremades, N. Aliaga-Alcalde and E. Ruiz, *J. Am. Chem. Soc.*, 2013, **135**, 7010–7018; (e) E. Colacio, J. Ruiz, E. Ruiz, E. Cremades, J. Krzystek, S. Carretta, J. Cano, T. Guidi, W. Wernsdorfer and E. K. Brechin, *Angew. Chem., Int. Ed.*, 2013, **52**, 9130–9134; (f) W. Huang, T. Liu, D. Wu, J. Cheng, Z. W. Ouyang and C. Duan, *Dalton Trans.*, 2013, **42**, 15326–15331; (g) R. Boča, J. Miklovič and J. Titiš, *Inorg. Chem.*, 2014, **53**, 2367–2369; (h) S. Gómez-Coca, A. Urtizberea, E. Cremades, P. J. Alonso, A. Camón, E. Ruiz and F. Luis, *Nat. Commun.*, 2014, **5**, 4300; (i) Y. -Y. Zhu, Y. -Q. Zhang, T. -T. Yin, G. Chen, B. -W. Wang and G. Song, *Inorg. Chem.*, 2015, **54**, 5475–5486; (j) V. V. Novikov, A. A. Pavlov, Y. V. Nelyubina, M.-E. Boulon, O. A. Varzatskii, Y. Z. Voloshin and R. E.P. Winpenny, *J. Am. Chem. Soc.*, 2015, **137**, 9792–9795.
- 11 (a) H. Miyasaka, K. Nakata, L. Lecren, C. Coulon, Y. Nakazawa, T. Fujisaki, K. Sugiura, M. Yamashita and R. Clérac, *J. Am. Chem. Soc.*, 2006, **128**, 3770–3783; (b) I. -R. Jeona and R. Clérac, *Dalton Trans.*, 2012, **41**, 9569–9586; (c) N. Nedelko, A. Kornowicz, I. Justyniak, P. Aleshkevych, D. Prochowicz, P. Krupiński, O. Dorosh, A. Ślawska-Waniewska and J. Lewiński, *Inorg. Chem.*, 2014, **53**, 12870–12876.
- 12 (a) Y. -Y. Zhu, M. -S. Zhu, T. -T. Yin, Y. -S. Meng, Z. -Q. Wu, Y. -Q. Zhang and G. Song, *Inorg. Chem.*, 2015, **54**, 3716–3718; (b) J. Palion-Gazda, T. Klemens, B. Machura, J. Vallejo, F. Lloret and M. Julve, *Dalton Trans.*, 2015, **44**, 2989–2992.
- 13 A. Aijaz, P. Lama, E. C. Saudo, R. Mishra and P. K. Bharadwaj, *New J. Chem.*, 2010, **34**, 2502–2514.
- 14 Y. -L. Wang, L. Chen, C. -M. Liu, Y. -Q. Zhang, S. -G. Yin and Q. -Y. Liu, *Inorg. Chem.*, 2015, **54**, 11362–11368.
- 15 (a) J. Zhang, S. Chen, A. Zingiryan and X. Bu, *J. Am. Chem. Soc.*, 2008, **130**, 17246–17247; (b) D. -S. Li, Y. -P. Wu, J. Zhao, J. Zhang, J. Y. Lu, *Coord. Chem. Rev.*, 2014, **261**, 1–27.
- 16 Y. -L. Wang, L. Chen, Q. -Y. Liu, Z. -Y. Du and Y. Yao, *CrystEngComm*, 2015, **17**, 7628–7631.
- 17 (a) T. Li, X. -J. Hong, X. Liu, R. Chen, Q. -G. Zhan, X. Xu, and Y. -P. Cai, *CrystEngComm.*, 2014, **16**, 3883–3889; (b) R. Mishra, M. Ahmad and M. R. Tripathi, *Polyhedron.*, 2013, **50**, 22–30.
- 18 (a) M.-H. Zeng, Z. Yin, Y. -X. Tan, W. -X. Zhang, Y. -P. He and M. Kurmoo, *J. Am. Chem. Soc.*, 2014, **136**, 4680–4688; (b) F. E. Mabbs and D. J. Machin, *Magnetism and Transition Metal Complexes*; Dover Publications: Mineola, NY, 2008; (c) X. C. Huang, C. Zhou, D. Shao and X. Y. Wang, *Inorg. Chem.*, 2014, **53**, 12671–12673; (d) J. M. Zadrozny, J. Liu, N. A. Piro, C. J. Chang, S. Hill and J. R. Long, *Chem. Commun.*, 2012, **48**, 3927–3929; (e) R. C. Poulten, M. J. Page, A. G. Algarra, J. J. Le Roy, I. López, E. Carter, A. Llobet, S. A. Macgregor, M. F. Mahon, D. M. Murphy, M. Murugesu and M. K. Whittlesey, *J. Am. Chem. Soc.*, 2013, **135**, 13640–13643.
- 19 M. Grahl, J. Kozler and I. Sessler, *J. Magn. Mater.*, 1990, **187**, 90–91.
- 20 M. Jeletic, P. H. Lin, J. J. L. Roy, I. Korobkov, S. I. Gorelsky, M. Murugesu, *J. Am. Chem. Soc.*, 2011, **133**, 19286–19289.
- 21 (a) J. Ruiz, A. J. Mota, A. Rodríguez-Diéguez, S. Titos, J. M. Herrera, E. Ruiz, E. Cremades, J. P. Costes and E. Colacio, *Chem. Commun.*, 2012, **48**, 7916–7918; (b) Y. -N. Guo, G. -F. Xu, P. Gamez, L. Zhao, S. -Y. Lin, R. Deng, J. Tang and H. -J. Zhang, *J. Am. Chem. Soc.*, 2010, **132**, 8538–8539.
- 22 O. Kahn. *Molecular Magnetism*; VCH: Weinheim, Germany, 1993.
- 23 Y. -L. Wang, J. -H. Fu, J. -J. Wei, X. Xu, X. -F. Li and Q. -Y. Liu, *Cryst. Growth Des.*, 2012, **12**, 4663–4668.
- 24 APEX2, SADABS and SAINT. Bruker AXS Inc.: Madison, Wisconsin, USA. 2008.
- 25 G. M. Sheldrick, *Acta Cryst.*, 2008, **A64**, 112–122.

### Graphical Abstract

A 3D chiral and a 2D achiral cobalt(II) compounds have been synthesized and characterized. Detailed magnetic measurements on **1** and **2** show field-induced slow magnetic relaxation resulting from single-ion anisotropy of the individual Co(II) ions in **1** and **2**. The different magnetic anisotropy energy barriers for **1** and **2** are resulted from the distinct coordination environments of Co(II) ions.

